Catalysis Today 161 (2011) 202–208

Contents lists available at ScienceDirect

Catalysis Today

journal homepage: www.elsevier.com/locate/cattod

A study into the self-cleaning surface properties—The photocatalytic decomposition of oleic acid

Jiří Rathouský[a,*], Vít Kalousek[a], Michal Kolář[a], Jaromír Jirkovský[a], Petr Barták[b]

[a] J. Heyrovský Institute of Physical Chemistry of AS CR, v.v.i., Dolejškova 3, 182 23 Prague 8, Czech Republic
[b] Department of Analytical Chemistry, Palacký University, Třída 17. listopadu 12, 771 46 Olomouc, Czech Republic

ARTICLE INFO

Article history:
Received 12 June 2010
Received in revised form 21 October 2010
Accepted 12 November 2010
Available online 8 December 2010

Keywords:
TiO_2
Mesoporous layers
Oleic acid
Photocatalysis
Mechanism of the oleic acid degradation
Self-cleaning surfaces

ABSTRACT

Thin films of TiO_2 exhibiting developed mesoporosity with large surface area and pores ca 10 nm in size were shown efficient photocatalyst in the decomposition of thin layers of oleic acid deposited on their surface. The pore walls of these films were composed of small anatase nanocrystals (ca 40–60%) and some amorphous phase. As major intermediates of the oleic acid decomposition, nonanal and 9-oxononanoic acid were identified. Azelaic and nonanoic acid were detected as well, representing minor intermediates. These compounds have been shown to correspond with the products of a simulated oxidative degradation of cis-3-hexenoic acid computed by means of quantum chemistry. Cis-3-hexenoic acid was chosen as a simplified model of oleic acid having similar but reduced structure. It enabled to perform the theoretical study with a reasonable consumption of computation time. The simulated oxidative degradation of cis-3-hexenoic acid was induced by an attack of hydroxyl radical on the C=C double bond. The main reaction pathway led to propanal, 3-oxopropanoic acid, and also hydroxyl radical. The organic products are analogous to the main degradation intermediates of oleic acid, nonanal and 9-oxononanoic acid. The prediction of hydroxyl radical elimination in the final step of the major reaction sequence would mean that it may act as a catalyst causing accelerated degradation of unsaturated compound including fatty acids.

1. Introduction

The requirement to render the surface of a number of products self-cleaning or at least easy-to-clean is an important general issue in a vast range of technologies. Such a distinguished property would substantially enhance the utility value of the products and would improve the environment quality. The soiling of the external surfaces of buildings and other constructions is a major issue in the environmental protection. One of the promising possibilities of the remedy is to cover their surface with a photocatalytically active finish. Such a coating should be active enough to decompose the solid or liquid deposits of dirt or to convert them to oxygenated organic compounds which can be easily washed off.

Due to its unique properties, the anatase crystalline films with developed 3D mesoporosity are photocatalysts of choice for the environmental applications [1–12]. In recent years, a generalized sol–gel procedure for the preparation of large-pore mesoporous films of metal oxides was developed. It is based on a mechanism combining evaporation-induced self-assembly (EISA) of a block copolymer with the complexation of molecular inorganic species, enabling the preparation of mesoporous films with good mechanical, optical and transport properties [13–15]. The latter property will ensure better transport of O_2 and H_2O, which are viable for the photocatalytic degradation of deposits. This transport is often significantly hindered by a compact layer of grease.

This study aims at the systematic investigation of photocatalytic performance of mesoporous layers of TiO_2 towards thin-layer deposits of oleic acid, serving as a model compound for fatty dirt, which were spread either by dip- or spray-coating, and treated at different temperatures. This systematic study provides a sound background for the development of self-cleaning finishes for a wide range of technologies.

Due to its properties (double bond, low volatility, liquidity at room temperature and stability in the condensed phase) and ample occurrence, oleic acid is a suitable model compound to simulate grease stains on various types of surfaces. Because of its double bond and influence on the mechanism of photocatalytic oxidation, oleic acid is more appropriate for the mentioned simulation than saturated fatty acids. Last but not least, it was suggested as a test molecule in the draft of international standard for testing the self-cleaning ability of surfaces. However, the mechanism of its photocatalytic decomposition has not been sufficiently elucidated

* Corresponding author. Tel.: +420 266053945; fax: +420 286582307.
E-mail address: jiri.rathousky@jh-inst.cas.cz (J. Rathouský).

0920-5861/$ – see front matter © 2010 Elsevier B.V. All rights reserved.
doi:10.1016/j.cattod.2010.11.030

yet. Therefore a special attention was devoted to a theoretical study into the mechanism in order to reveal the major reaction pathways.

2. Experimental

2.1. Film preparation and characterization

Mesoporous films of TiO_2 were prepared according to the following procedure: the reaction mixture contained 14.4 mL of titanium (IV) ethoxide, 56 mL of 1-butanol, 10.2 mL of HCl and 5 g of Pluronic P123 (BASF). The films were deposited by dip-coating glass slides at a withdrawal rate of 1.5 mm/s at relative humidity of 20%. Afterwards the films were aged at room temperature for 24 h and calcined in air at 350 °C for 3 h. In order to obtain thicker films, the procedure was repeated. All the chemicals were obtained from Sigma–Aldrich (except for the Pluronic template).

The morphological properties of the films were obtained by combining several techniques. The surface relief of the films was revealed by atomic force microscopy (AFM) using a Digital Instruments NanoScope apparatus. The details of the surface texture were provided by high-resolution scanning electron microscopy using a Jeol JSM-6700 F apparatus and high resolution transmission electron microscopy (HR-TEM Jeol JEM-2100F UHR). The crystallinity was assessed by X-ray diffraction using a Siemens D 5005 diffractometer in the Bragg–Brentano geometry using CuKα radiation. The thickness of the films was measured using a Sopralab ellipsometer.

The absorption spectra of mesoporous films were obtained with a Perkin Elmer Lambda 19 spectrophotometer equipped with an integration sphere. First, transmitance (T) and reflectance (R) spectra of a glass slide with a thin film were measured. Then, the corresponding absorption spectrum (A) was calculated using the formula $A = 1 - T - R$. Finally, the absorbance spectrum (OD) was obtained employing the relation $OD = -\log(1 - A)$. The absorbance of a thin film at a particular wavelength was determined as a difference between the absorbance of a glass slide with and without a film.

The texture properties of the films were determined by the analysis of adsorption isotherms of Kr at 77 K using a Micromeritics ASAP 2010 volumetric adsorption unit.

2.2. Photocatalytic testing

Prior to the photocatalytic experiments, the test pieces were cleaned using UV light irradiation (2 mW/cm^2) for 24 h. Oleic acid was deposited either by dip-coating from its 10% heptane solution at the withdrawal rate of 1 mm/s or the heptane solution was sprayed on a surface preheated at 70 °C. Afterwards the films were dried at 70 °C for 15 min.

The photocatalytic decomposition of oleic acid due to UV radiation (Sylvania Lynx-S 11W BLB lamps, 365 nm, 2.0 mW/cm^2) was followed by measuring the contact angle for water, which can be expected proportional to the degree of its degradation, i.e., its transformation into more hydrophilic compounds as well as to gaseous products (CO_2, H_2O), which leads to the exposure of the hydrophilic TiO_2 surface. Parallel the sample mass in the course of irradiation was measured. However, the interpretation of changes in mass is ambiguous, as two opposite processes are occurring, namely a decrease in mass due to the transformation of oleic acid into gaseous products and an increase due to the transformation into more oxygenated products.

2.3. Detection of intermediate products

After the irradiation, the layers were rinsed with heptane. In course of irradiation, the volatile components were captured by the solid phase microextration method (SPME) using a Supelco fibre with carboxen/PDMS phase placed in the vicinity of the layer for 1 h. The extracts and adsorbed molecules were analyzed by GC–MS, performed on HP 6890 GC system with HP 7683 injector equipped with an Agilent 5973 N mass selective detector. Helium was flowing through a ZB5-MS column (30 m × 0.25 mm, 0.25 μm) at a rate of 0.9 mL min^{-1}. Temperature in the oven increased from 40 to 250 °C at the rate of 5 °C min^{-1} with 2 min of isothermal section at the beginning of the analysis. MS scans were recorded within the range of 29–370 m/z using EI ionization (energy 70 eV).

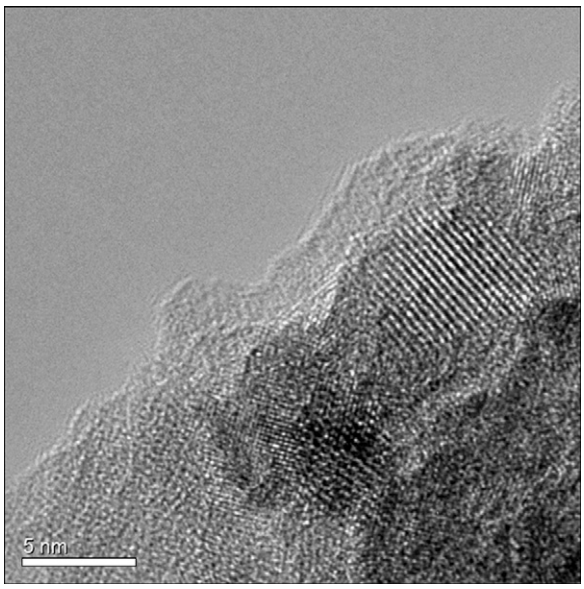

Fig. 1. TEM image of a typical one-layer mesoporous film of TiO_2.

3. Results and discussion

3.1. Morphological and structure properties of mesoporous films

The AFM relief of the prepared films was very flat without height variations in excess of ca 10 nm. The pore openings are relatively regularly distributed within the surface with an average size of ca. 8 nm. The TEM and SEM images show more or less regularly ordered pores, whose size ranges from 8 to 10 nm (Fig. 1). The pores were separated by walls about 3–4 nm in thickness. The thickness of one- and two-layer films equalled in average 320 and 650 nm, respectively.

Powder X-ray diffractograms of the mesoporous films showed the presence of only one crystalline phase – anatase. The presence of an X-ray amorphous titania component is the probable reason why the X-ray diffractograms showed decreased intensity of reflections due to anatase in comparison with a reference fully crystalline material prepared by the destruction of the mesoporous film by calcination at 600 °C.

UV/VIS absorption spectra of the one and two-layer mesoporous films showed some blue shift in the comparison with a bulk TiO_2 (absorption threshold of 388 nm). The difference of the spectra for one- and two-layer films is due to their different thickness. The repeated calcination could also lead to certain increase in the size of the anatase nanocrystals and the formation of some lattice defects.

From the transmission spectra the optical band gap (E_g) can be calculated using the relation

$$\alpha h\nu = A(h\nu - E_g)^n, \quad (1)$$

where α is the absorption coefficient, A the constant [16]. For the anatase polymorph of TiO_2, the optical transition is indirect, with

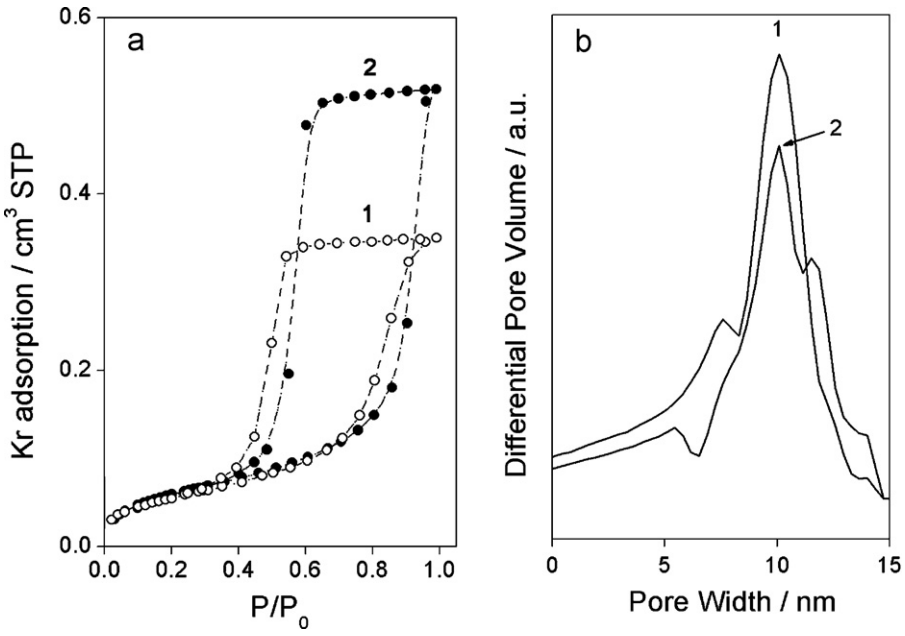

Fig. 2. Adsorption isotherms of Kr at 77 K (a) on one-layer (1) and two-layer (2) films and the corresponding pore size distribution (b).

the exponent $n = 2$. Furthermore, in the region of strong absorption, and at normal incidence, the reflectivity is very low and can be neglected [17]. This leads to the following expression for the absorption coefficient α as a function of transmittance T

$$\alpha = -2.303\frac{\log T}{t} \quad (2)$$

where t is the film thickness [14]. Eq. (1) then becomes $-2.303h\nu \log T = B(h\nu - E_g)^2$, and the slope of $(-2.303h\nu \log T)^{1/2}$ vs $h\nu$ provides a linear section that can be extrapolated to zero, providing E_g. The resulting optical band gap energies E_g were estimated 3.34 and 3.33 eV for the one- and two-layer films, respectively. For all the films the band gap is substantially wider than that of bulk anatase of ca 3.2 eV, indicating the nanoparticle structure of the pore walls.

In order to determine the texture parameters of thin porous films deposited on supports, whose geometrical surface area is as small as several tens of square centimetres only, a high-sensitive Kr adsorption technique has to be used. The most frequently used adsorptives, namely, nitrogen and argon at ca 77 and 87 K, respectively, cannot be applied with materials with very small surface areas. The saturation pressures of nitrogen and argon at 77 and 87 K, respectively, reach ca. 760 Torr, which leads to an extremely large number of molecules being trapped within the void volume of the sample cell. Because of a very small total pore volume and surface area of such thin porous films, the pressure changes due to the adsorption cannot be measured with a sufficient precision. As an alternative, an adsorptive with a substantially lower saturation vapour pressure should be used, such as krypton at the boiling point of liquid nitrogen.

The information on the pore size and pore volume can be obtained from Kr isotherms by analyzing the shape of their hysteresis loop and the limiting adsorption at saturation pressure as well as by comparison of the adsorption on the samples under study with that on well-defined reference materials (Fig. 2a). A geometric area of 1 cm^2 of the one- and two-layer films showed the BET surface area of 147 and 273 cm^2, respectively. Similarly, the total pore volume (also related to a geometric area of 1 cm^2) calculated from the limiting adsorption equals 0.0275 and 0.0469 mm^3, respectively. From the thickness of the film and the total pore volume the porosity of both one- and two-layer films was calculated, equalling 41 and 37%.

As the analysis of adsorption isotherms of Kr at 77 K providing the pore size distribution is far from being straightforward and a well-established procedure (e.g. DFT) has not been implemented yet, a simple method based on comparative plots was used [17,18]. As a suitable reference material a non-porous anatase (Aldrich, 11.2 m^2/g) was used. Comparison plots for both samples were constructed, in which the adsorption on the sample under study was plotted against that on the reference material. The differentiation of obtained plots provided an assessment of the pore size distribution for each film (Fig. 2b). A comparison of the texture properties of powders determined by the theoretical DFT analysis of nitrogen isotherms at 77 K with the krypton data provided a linear correlation between the standard adsorption and the pore size, and proved the closeness of nitrogen and krypton data. This correlation was used to scale the x-axis. Fig. 2b shows that the pore size distribution for both one- and two-layer films is rather narrow, being centred at ca 10 nm.

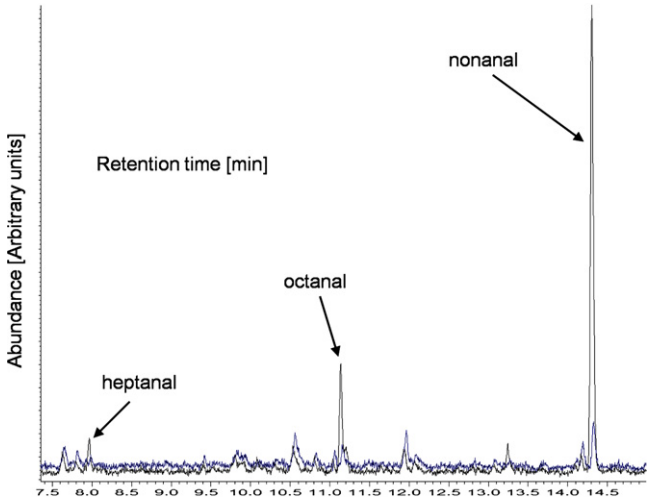

Fig. 3. GC chromatogram of oleic acid degradation intermediates captured by SPME (vs blank).

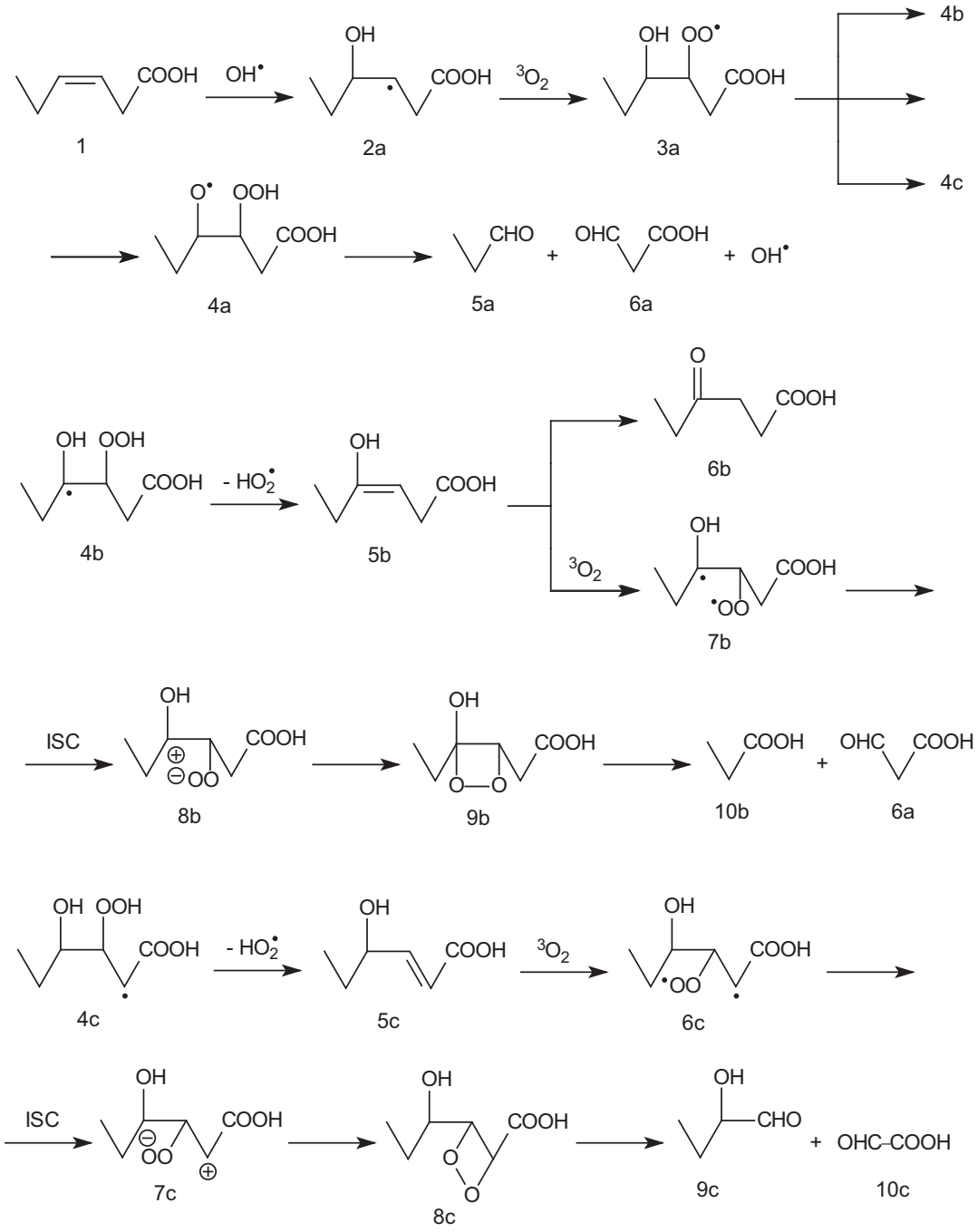

Fig. 4. Reaction scheme of oxidative degradation of cis-3-hexenoic acid induced by attack of hydroxyl radical onto carbon atom in position 4.

All the provided experimental data clearly proved that the films showed developed mesoporosity with large surface area and more or less regularly ordered pores ca 10 nm in size. The pore walls were composed of small anatase nanocrystals (ca 40–60%) and some amorphous phase.

3.2. Mechanism of oleic acid degradation

While the mechanism of photodegradation of oleic acid on TiO_2 has not been described yet, its reaction with ozone has been studied [19,20]. As primary and secondary intermediates, nonanal and 9-oxononanoic acid, and azelaic and nonanoic acid were detected, respectively.

In the present study, nonanal and 9-oxononanoic acid were identified as the main intermediates of the photocatalytic degradation of oleic acid. Azelaic acid and nonanoic acid were detected as well, however in smaller amount. Besides, traces of decanal, octanal and heptanal were identified using SPME extraction (Fig. 3).

To propose probable reaction pathways leading to the identified intermediates, quantum-chemical calculations with cis-3-hexenoic acid were performed using a Gaussian 09W software applying DFT B3LYP/6-31G(d) method. This molecule was chosen as a simplified model of oleic acid. Both substances contain cis –CH=CH– double bond as well as CH_3–, –CH_2– and –COOH groups. Their structures differ only in the number of methylene groups (oleic acid has 14 while cis-3-hexenoic acid 2). However,

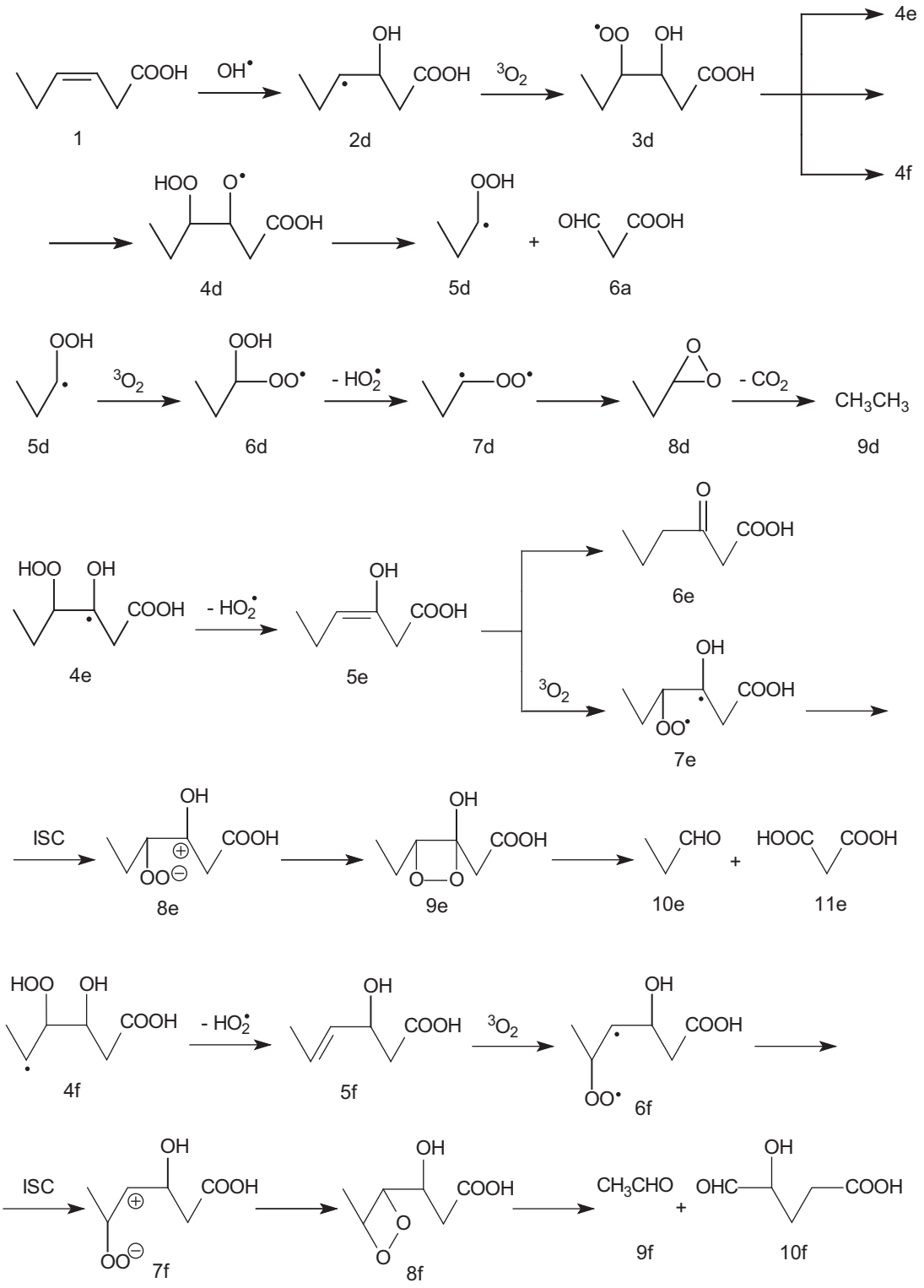

Fig. 5. Reaction scheme of oxidative degradation of cis-3-hexenoic acid induced by attack of hydroxyl radical onto carbon atom in position 3.

this difference is crucial regarding the feasibility of corresponding computations that would take enormously long time for oleic acid but were executable within a reasonable time for cis-3-hexenoic acid. Nevertheless, some of the results found for the model compound are valid to the whole homologous series, including oleic acid.

The performed computations concerned reactions that possibly occur in the course of an oxidative degradation of cis-3-hexenoic acid induced by an attack of hydroxyl radical. The proposed reaction mechanism is presented in Figs. 4 and 5.

Quantum chemical method was applied to particular reactions of the proposed mechanism to confirm their feasibility. A typical procedure started with the search of the transition states that could connect particular reactants and products. After the transition structure was found and optimized, the corresponding reaction coordinate was computed to verify that it really connects the start-

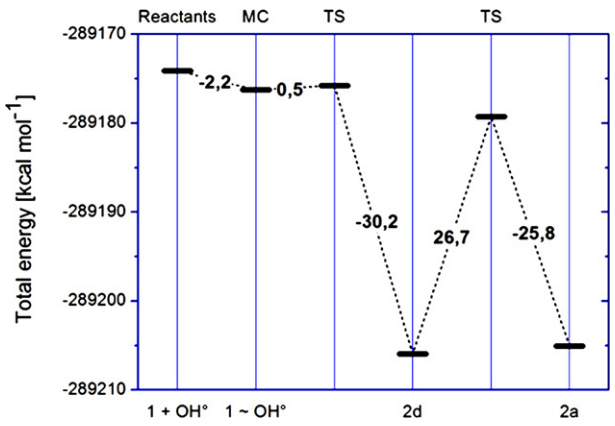

Fig. 6. Energy diagram of interaction of hydroxyl radical with cis-3-hexenoic acid producing two isomeric OH-adducts (2d and 2a).

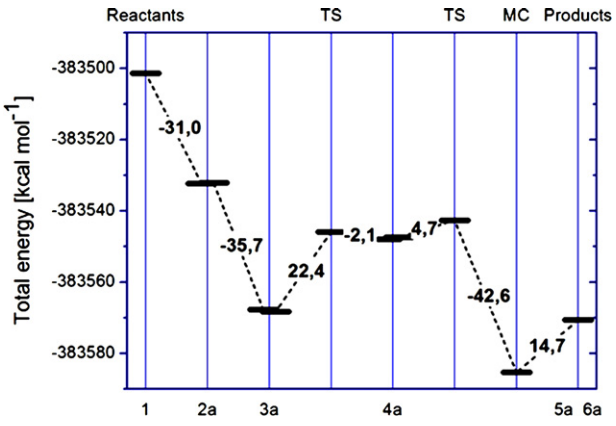

Fig. 8. Energy diagram of the main pathway of oxidative degradation of cis-3-hexenoic acid (1) to propanal (5a) and 3-oxopropanoic acid (6a).

ing and final structures. Finally, activation and reaction energies were calculated by comparing zero-point corrected energies of the reactants, products and transition states.

First, an interaction of hydroxyl radical with cis-3-hexenoic acid and its addition onto double bond were investigated. The results are summarized in the energy diagram in Fig. 6.

A weak molecular complex exists between cis-3-hexenoic acid (1) and hydroxyl radical (OH•). The distances between hydroxyl oxygen atom and double bond carbons are 2.92 Å (C3) and 3.49 Å (C4), respectively. A very low activation energy of 0.5 kcal/mol is enough to overcome transition state (TS) and form an OH-adduct hydroxylated on carbon in position 3 (2d). The transfers of OH group between positions 3 and 4 require activation energies around 26 kcal/mol whereas hydroxyl in position 3 is slightly favoured.

The odd electron can formally move along the carbon chain (Fig. 7). It is realized by transfers of corresponding hydrogen atoms. The calculated activation energies of these H-transfers are relatively high, ranging between 35 and 50 kcal/mol. That is why subsequent addition of triplet oxygen dominates because it runs spontaneously without any energy barrier. The formed peroxyl radicals tend to abstract hydrogen atom from neighbouring positions. It was found that hydrogen of hydroxyl group is preferable to the carbon hydrogens. While activation energies of the reactions 3a–4a and 3d–4d are 20.4 and 22.4 kcal/mol, those of 3a–4b and 3d–4e are higher 28.8 and 34.8 kcal/mol, respectively. Products of the former reactions (4a and 4d) undergo an easy splitting of C–C bond giving rise to propanal (5a), 3-oxopropanoic acid (6a) and, for the reaction sequence 1–2a–3a–4a–5a and 6a, also hydroxyl radical. The corresponding energy diagram is shown in Fig. 8.

These compounds correspond with the main products of photocatalytic degradation of oleic acid, i.e., nonanal and 9-oxononanoic acid. The eliminated hydroxyl radical could act catalytically and thus cause accelerated degradation of unsaturated compound

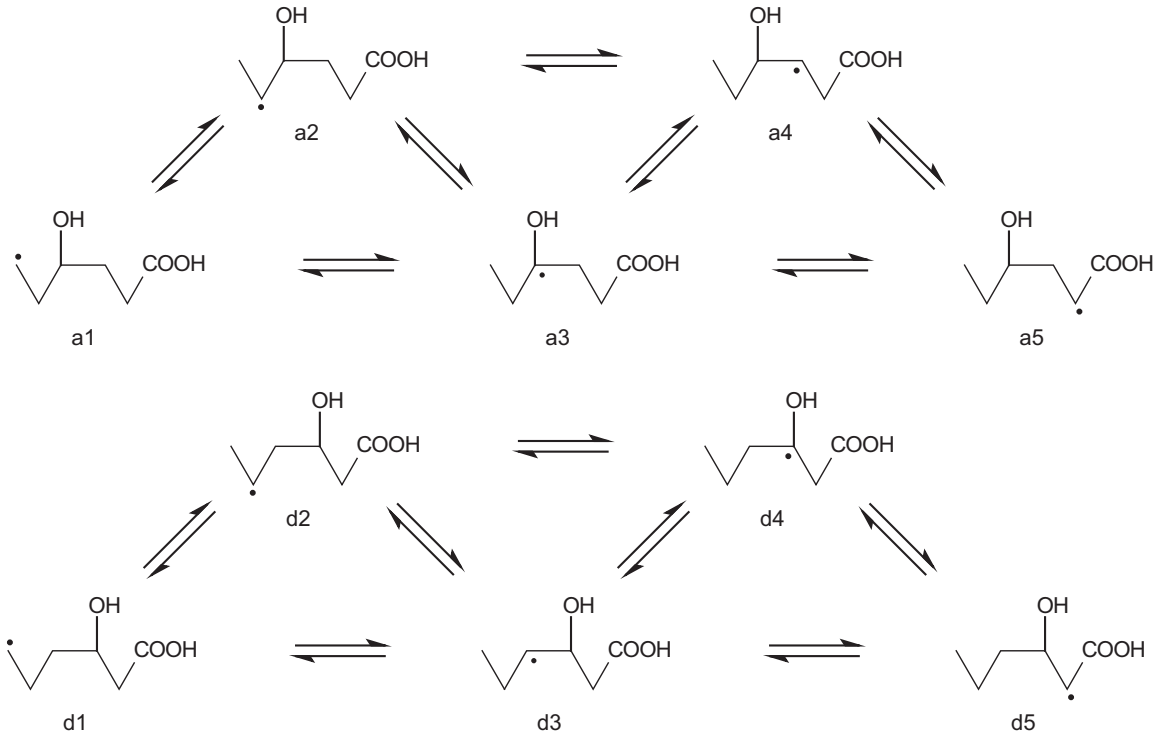

Fig. 7. Reaction schemes of transfers of hydrogen atoms along or across the carbon chain in two isomeric OH-adducts of cis-3-hexenoic acid (2a and 2d).

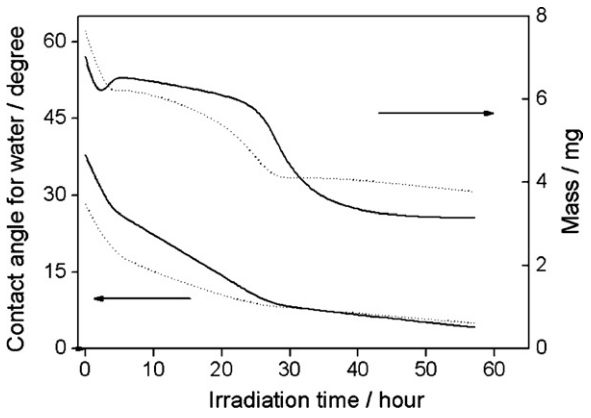

Fig. 9. Time evolution of contact angle for water and mass of oleic acid deposited on one-layer TiO_2 film during the irradiation with UV light. Oleic acid was deposited by spraying its 5% heptanes solution. Dotted and solid lines show two independent experiments for different amount of deposited oleic acid.

including fatty acids. Further results of the theoretical study will be described in detail in a separate article.

3.3. Photocatalytic performance followed by the contact angle measurement

Photocatalytic experiments were aimed on the assessment of the effect of the thickness of the mesoporous film of TiO_2 and the mass and way of the deposition of oleic acid on the photocatalytic performance. Two different methods used for the spreading of oleic acid provide deposits with completely different character, namely its smooth and uniform layer by dip-coating or more or less interconnected droplets by spraying. These two variants could simulate different situations which can occur in real applications.

Firstly, the photocatalytic performance of one- and two-layer TiO_2 films was compared, the oleic acid being deposited by dip-coating from its 5% heptane solution. Both TiO_2 films exhibited a fast decrease in the contact angle for water corresponding to the high rate of the photocatalytic transformation of oleic acid. At shorter irradiation times, the degradation proceeded faster on two-layer TiO_2 film. In the case of higher concentrations of oleic acid (10%) in its heptane solution used for dip-coating, the decrease in the contact angle for water was slower. However, even for the larger amount of the deposited oleic acid the performance of the two-layer TiO_2 film was only slightly worse.

The photocatalytic degradation of oleic acid deposited by spraying on one-layer TiO_2 film was followed also by a gravimetric method (Fig. 9). During 30 h of irradiation, the mass of the organic layer was gradually decreasing. A major decrease in mass occurred within the first 20 h that correlates well with the contact angle measurements.

To assess the limits of the photocatalysis on mesoporous layers of TiO_2, also the degradation of partly carbonized layers of oleic acid was attempted, which is of course much more difficult. The complete removal was possible only for thinner carbonized layers. Thicker layers could not be removed even after prolonged UV irradiation, probably due to their very limited UV transparency. However, we found that the efficiency of removal was enhanced by higher humidity and temperature during the photocatalytic process, especially in the saturated water vapour at 60 °C. The water vapour seems to have twofold beneficial effects, namely an increased photogeneration of OH radicals responsible for the primary attack on the organic matter as well as the break-up of the compactness and lowering the adhesion of the carbonized layer, which can be due to both liquid water and its vapour at higher temperatures.

4. Conclusion

The carried out photocatalytic experiments showed that mesoporous TiO_2 films with large surface area and pores of ca 10 nm in size are efficient photocatalyst in the decomposition of thin layers of oleic acid deposited by dip- or spray-coating on their surface and are therefore possible candidates for self-cleaning coatings. While nonanal and 9-oxononanoic acid were identified as primary intermediates of the photocatalytic degradation of oleic acid, azelaic acid and nonanoic acid were the secondary intermediates. These compounds have been shown to correspond with the main products determined by quantum mechanical calculations of photocatalytic degradation of model cis-3-hexenoic acid. In these calculations the oxidative degradation was induced by an attack of hydroxyl radical on the double bond. It has been found that the eliminated hydroxyl radical could act catalytically and thus cause accelerated degradation of unsaturated compound including fatty acids.

Acknowledgement

The authors are thankful to the Grant Agency of the Czech Republic (grants no. 104/08/0435-1 and 203/08/H032) and to the Ministry of Education, Youth and Sport of the Czech Republic (project 1M0577).

References

[1] F. Bosc, A. Ayral, C. Guizard, Thin Solid Films 495 (2006) 252.
[2] F. Bosc, D. Edwards, N. Keller, V. Keller, A. Ayral, Thin Solid Films 495 (2006) 272.
[3] E. Allain, S. Besson, C. Durand, M. Moreau, T. Gacoin, J.P. Boilot, Adv. Funct. Mater. 17 (2007) 549.
[4] Y. Sakatani, D. Grosso, L. Nicole, C. Boissiere, G.J. de, A.A. Soller-Illia, C. Sanchez, J. Mater. Chem. 16 (2006) 77.
[5] A. Mills, G. Hill, S. Bhopal, I.P. Pakin, S.A. O'Neil, J. Photochem. Photobiol. A 160 (2003) 185.
[6] J.C. Yu, X. Wang, X. Fu, Chem. Mater. 16 (2004) 1523.
[7] J. Tang, Y. Wu, E.W. McFarland, G.D. Stucky, Chem. Commun. (2004) 1670.
[8] M. Andersson, H. Birkedal, N.R. Franklin, T. Ostomel, S. Boettcher, A.E.C. Palmquist, G.C. Stucky, Chem. Mater. 17 (2005) 1409.
[9] H. Wang, J.J. Miao, J.M. Zhu, H.M. Ma, J.J. Zhu, H.Y. Chen, Langmuir 20 (2004) 11738.
[10] M. Wark, J. Tschirch, O. Bartels, D. Bahnemann, J. Rathouský, Microporous Mesoporous Mater. 84 (2005) 247.
[11] J. Rathouský, D. Fattakhova-Rohlfing, M. Wark, T. Brezesinski, S. Smarsly, Thin Solid Films 515 (2007) 6541.
[12] J. Tschirch, D. Bahnemann, M. Wark, J. Rathouský, J. Photochem. Photobiol. A 194 (2008) 181.
[13] P. Yang, D. Zhao, D.I. Margolese, B.F. Chmelka, G.D. Stucky, Nature 396 (1998) 152.
[14] C.J. Brinker, Y.F. Lu, A. Sellinger, H.Y. Fan, Adv. Mater. 11 (1999) 579.
[15] C. Sanchez, C. Boissiere, D. Grosso, C. Laneryty, L. Nicole, Chem. Mater. 20 (2008) 682.
[16] J. Tauc, Optical Properties of Solids, Academic Press, New York, 1966, 277–313.
[17] J. Rathouský, V. Kalousek, C. Walsh, A. Bourgeois, in: Book of Abstracts 5th International Workshop "Characterization of Porous Materials: From Angstroms to Millimeters", New Brunswick, 2009.
[18] J. Rathouský, V. Kalousek, V. Yarovyi, M. Wark, J. Jirkovský, J. Photochem. Photobiol. A: Chem. 216 (2010) 126.
[19] H.-M. Hung, P. Ariya, J. Phys. Chem. A 111 (2007) 620.
[20] Y. Katrib, S.T. Martin, H.-M. Hung, Y. Rudich, H. Zhang, J.G. Slowik, P. Davidovits, J.T. Jayne, D.R. Worsnop, J. Phys. Chem. A 108 (2004) 6686.